

RESEARCH ARTICLE | AUGUST 01 2022

Spectroscopic identification and characterization of the aluminum methylene (AlCH_2) free radical

Fumie X. Sunahori ; Tony C. Smith ; Dennis J. Clouthier  



J. Chem. Phys. 157, 044301 (2022)

<https://doi.org/10.1063/5.0101060>



Articles You May Be Interested In

Ab initio spectroscopy of the aluminum methylene (AlCH_2) free radical

J. Chem. Phys. (July 2020)

Spectroscopic detection of the gallium methylene (GaCH_2 and GaCD_2) free radical in the gas phase by laser-induced fluorescence and emission spectroscopy

J. Chem. Phys. (January 2024)

A revised nuclear quadrupole moment for aluminum: Theoretical nuclear quadrupole coupling constants of aluminum compounds

J. Chem. Phys. (June 2019)



The Journal of Chemical Physics

Special Topics Open for Submissions

[Learn More](#)

Spectroscopic identification and characterization of the aluminum methylene (AlCH₂) free radical

Cite as: J. Chem. Phys. 157, 044301 (2022); doi: 10.1063/5.0101060

Submitted: 28 May 2022 • Accepted: 29 June 2022 •

Published Online: 1 August 2022



View Online



Export Citation



CrossMark

Fumie X. Sunahori,¹ Tony C. Smith,² and Dennis J. Clouthier^{2,a)}

AFFILIATIONS

¹Department of Chemistry and Biochemistry, Rose-Hulman Institute of Technology, 5500 Wabash Ave., Terre Haute, Indiana 47803, USA

²Ideal Vacuum Products, LLC, 5910 Midway Park Blvd. NE, Albuquerque, New Mexico 87109, USA

^{a)}Author to whom correspondence should be addressed: djc@idealvac.com

ABSTRACT

The AlCH₂ free radical has been spectroscopically identified for the first time. This highly reactive species was produced in an electric discharge jet using trimethylaluminum vapor in high pressure argon as the precursor. The laser-induced fluorescence spectrum of the $\tilde{B}^2A_2 - \tilde{X}^2B_1$ band system in the 513–483 nm region was recorded, and the 0–0 bands of AlCH₂ and AlCD₂ were studied at high resolution. The fine structure splittings were found to be due primarily to the Fermi contact interaction in the excited state rather than the usual spin–rotation coupling. Rotational analysis gave the molecular constants of the combining states, and the geometries were obtained as $r''(A1 - C) = 1.959(1) \text{ \AA}$, $r''(C - H) = 1.106(1) \text{ \AA}$, $\theta''_{\text{HCH}} = 110.4(1)^\circ$ and $r'(A1 - C) = 1.943(1) \text{ \AA}$, $r'(C - H) = 1.091(1) \text{ \AA}$, $\theta'_{\text{HCH}} = 115.4(1)^\circ$. The bond lengths correspond to an aluminum–carbon single bond in both states.

Published under an exclusive license by AIP Publishing. <https://doi.org/10.1063/5.0101060>

I. INTRODUCTION

The aluminum methylene or AlCH₂ free radical has not hitherto been identified spectroscopically, despite its potential significance in several areas of chemistry. Aluminum is the most abundant metal (8% by weight) in the earth's crust and the third most abundant element after oxygen and silicon. Its light weight, low cost, corrosion resistance, ease of fabrication, and variety of useful alloys make it indispensable in industries ranging from transportation to packaging, electrical applications to construction, and machinery to household items. Organoaluminum compounds, typified by trimethylaluminum (TMA) (which exists primarily in dimeric form), are one of the major themes in organometallic chemistry and are extensively used as catalysts for alkene polymerization processes. Coordinately unsaturated organoaluminum species are thought to play key roles in homogeneous and heterogeneous catalysis although few such entities have been identified spectroscopically. In this sense, simple radicals, such as AlCH, AlCH₂, and AlCH₃, are fundamental building blocks in organoaluminum chemistry.¹

Furthermore, it has been argued that AlCH₂ has significant potential to be an interstellar molecule.² Aluminum has the highest cosmic abundance among metals,³ methylene has been detected in

the interstellar medium (ISM),⁴ and the simple methylenic species H₂CN, H₂CO, and H₂CS are prominent interstellar molecules.⁵ In addition, five aluminum-containing molecules AlF, AlCl, AlO, AlOH, and AlNC have already been detected in the circumstellar envelope of IRC+10216 or VY Canis Majoris.⁵ Theoretical calculations predict the dipole moment of AlCH₂ necessary for microwave observations to be significant (0.8 D) and that AlCH₂ is thermodynamically stable with respect to dissociation to fragmentation to triplet methylene and an aluminum atom ($\Delta H_{0K} = +83.57 \text{ kcal/mol}$).² Experimentally, Srinivas *et al.*⁶ have used neutralization-reionization mass spectrometry (NRMS) to show that AlCH₂ and AlCH₃ are viable species in the gas phase, which do not show any evidence of isomerization to the corresponding hydridoaluminum species (HAlCH and HAlCH₂). All indications are if the microwave spectrum of AlCH₂ were known, radio astronomy searches for it in the ISM would be fruitful.

Although experimental data on AlCH₂ are limited to the single NRMS observation,⁶ the properties of the radical have been studied theoretically many times, beginning with early self-consistent field/double zeta plus polarized basis set (SCF/DZP) work of Fox *et al.*⁷ (on AlCH, AlCH₂, and AlCH₃) in 1980, who showed that aluminum prefers a $3s^2 3p$ configuration and forms an

aluminum–carbon single bond. Shortly thereafter, Cook and Allen⁸ qualitatively explained why $B=CH_2$ has a double bond but $Al-CH_2$ has a single bond due to the relative energetics of the boron and aluminum valence orbitals. Thus, the boron $2s$ and $2p$ orbitals are energetically sufficiently close to those of CH_2 to form a double bond but the $3s$ and $3p$ atomic orbitals of aluminum are higher in energy, which hinders such mixing so that both $AlCH_2$ and $AlCH$ have aluminum–carbon single bonds.⁹ In 1990 and 1991, Jin *et al.* reinvestigated the simple organoaluminum species at incrementally higher levels of theory.^{9,10} In 1991, Cramer¹¹ reported the *ab initio* predictions of the structures and isotropic hyperfine coupling constants of a variety of aluminum-containing free radicals, including $AlCH_2$. In 2013, Compaan *et al.* again considered the structure, spectroscopic constants, and vibrational frequencies of $AlCH_2$ with the aim of providing highly reliable properties that could be used as an aid to detecting the radical in outer space.² They also showed that the aluminum methylene structure was the lowest isomer on the potential energy surface. In an Appendix, the authors noted that the effect of core correlation appeared substantial in the prediction of the ground state vibrational frequencies, with differences calculated at the frozen-core and all-electron MP2 level of theory of a minimum of 7 cm^{-1} for the asymmetric CH stretch to maxima of 138 and 152 cm^{-1} for the AlC stretching and CH_2 scissoring vibrations, respectively. These discrepancies suggest that $AlCH_2$ is perhaps more complicated theoretically than previously suspected, despite the rather large body of *ab initio* studies.

Very recently, Tarroni and Clouthier¹² used high level *ab initio* theory to predict the properties of the ground and several excited electronic states of $AlCH_2$ and $AlCD_2$. They were able to show that previous difficulties with obtaining consistent predictions of the vibrational frequencies were not due to core correlation complications but rather to SCF instability of the single reference wavefunction. Internally contracted multireference configuration interaction (ICMRCI) calculations were used to predict the electronic spectra of the jet-cooled aluminum methylene radicals under typical laboratory conditions as an aid to their detection by laser spectroscopy. We now report experiments that have been successful in producing $AlCH_2$ and $AlCD_2$ in the gas phase, detection of the jet-cooled radicals by laser induced fluorescence, and the determination of the molecular properties of these interesting species from their spectra.

II. EXPERIMENT

The $AlCH_2$ and $AlCD_2$ radicals were generated by seeding the vapor of trimethylaluminum (TMA) into high pressure argon and subjecting pulses of this gas mixture to an electric discharge. As described in detail elsewhere,^{13,14} a pulsed molecular beam valve (General Valve, series 9) injected the precursor mixture into a flow channel where an electric discharge between two stainless steel ring electrodes fragmented the TMA, producing the species of interest and a variety of other products. The reactive intermediates were rotationally and vibrationally cooled by free jet expansion into vacuum at the exit of the pulsed discharge apparatus. A 1.0 cm long reheat tube¹⁵ added to the end of the discharge apparatus increased production of the $AlCH_2$ radicals and suppressed the background glow from excited argon atoms.

Since Clouthier *et al.* had already succeeded in detecting AlC, AlC_2 , and AlCCH by discharge jet spectroscopy of

trimethylaluminum,^{16–18} and our calculations¹² predicted several electronic transitions of $AlCH_2$ throughout the visible and ultraviolet, we determined that it would be necessary to survey the discharge products over a very broad range using all the tools at our disposal. For this purpose, we employed a versatile and highly sensitive 3D LIF spectrometer developed in the laboratory at Ideal Vacuum Products. The products of the TMA discharge were interrogated with the horizontally propagating laser beam of a broadly tunable optical parametric oscillator (Continuum Horizon OPO, $400\text{--}710\text{ nm}$, linewidth $3\text{--}7\text{ cm}^{-1}$, and energy $10\text{--}50\text{ mJ/pulse}$), and any resulting fluorescence was imaged vertically upward through appropriate long pass filters onto the photocathode of a red sensitive photomultiplier (RCA C31034A PMT). At the same time, fluorescence in the downward direction was collected with a lens and imaged onto the slit of a scanning monochromator (Spex 500 M) equipped with a 1200 line/mm grating blazed at 400 nm (in the red, 300 or 600 l/mm gratings both blazed at 500 nm were employed). The dispersed fluorescence was detected with an intensified, gated CCD detector (Andor iStar 320T, wavelength range of photocathode $280\text{--}760\text{ nm}$). The OPO was calibrated with simultaneously recorded neon optogalvanic lines and the monochromator with argon emission lines from a hollow cathode lamp.

At each laser step, the 3D LIF spectrometer recorded three dimensions of data: the complete total fluorescence decay curve (typically over $10\text{ }\mu\text{s}$), the laser wavelength, and the dispersed emission spectrum of the resulting fluorescence as follows: the PMT output current was digitized with $50\text{ }\Omega$ termination using a Tektronix MSO54 oscilloscope, triggered by the laser pulse detected by a photodiode. The digital signal was averaged ($100\text{--}500$ laser shots) and stored in our data acquisition computer. Scattered laser light was suppressed by one of the ten long pass filters mounted in a motorized filter wheel (ThorLabs CFW 3-10) and a computer selected as the laser scanner. At the same time, the emission spectrum was recorded at each fixed laser wavelength by accumulating the signal on the CCD, gated $6\text{--}8\text{ ns}$ after the laser pulse out to $\sim 8\text{ }\mu\text{s}$, for the same number of laser shots as the LIF average. Once the averaging was complete, the emission spectrum was read from the CCD and stored in the computer. At that point, the laser was moved to the next position (typically $2\text{--}3\text{ cm}^{-1}$ to the blue of the previous point), the monochromator was moved a similar amount to the blue to keep a constant offset (in cm^{-1} units) between the laser and the emission spectrum, and the averaging process was repeated. The range of each scan was limited by the number of available filters in each filter wheel and was typically $4000\text{--}5000\text{ cm}^{-1}$. The 3D spectra were wavenumber calibrated and concatenated to provide a continuous record of the LIF activity throughout the operational region of the OPO. By suitable mixing and doubling schemes, the wavelength region could be expanded, out to the CCD limit of 850 nm . The laser-induced fluorescence, emission, and calibration spectra were digitized and recorded simultaneously on a homebuilt computerized data acquisition system.

In practice, the 3D spectra were displayed as a color 2D plot of laser wavelength vs dispersed fluorescence intensity as a function of displacement from the laser or the laser wavelength vs total fluorescence intensity as a function of time. By suitably gating on time or dispersed fluorescence windows, spectra of different molecules or different transitions could be isolated and quickly identified from the rather massive datasets.

Moderate resolution (0.1 cm^{-1}) survey LIF spectra were recorded using a neodymium: yttrium aluminum garnet (Nd:YAG) pumped dye laser (Lumonics HD-500) excitation source in the same apparatus as described previously. The spectra were calibrated with optogalvanic lines from various argon- and neon-filled hollow cathode lamps to an estimated absolute accuracy of 0.1 cm^{-1} . Higher resolution ($\sim 0.04\text{ cm}^{-1}$ FWHM) LIF spectra were obtained using a narrow band (0.035 cm^{-1}) dye laser (Lambda-Physik Scanmate) as the excitation source using C500 dye. Absolute wavelength calibration of the dye laser, to an estimated accuracy of $\sim 0.003\text{ cm}^{-1}$, was performed by simultaneously recording the iodine LIF spectrum.¹⁹

For emission spectroscopy, previously measured LIF band maxima were excited by one of the dye lasers, and the resulting fluorescence was imaged with $f/4$ optics onto the entrance slit of a 0.5 m scanning monochromator (Spex 500M). The emission spectra were calibrated to an estimated accuracy of $\pm 1\text{ cm}^{-1}$ using emission lines from an argon-filled hollow cathode lamp. A 1200 line/mm grating blazed at 400 nm was employed in this work, which gave a bandpass of 29.9 nm with an 18 mm effective active area on the CCD.

Trimethylaluminum [TMA or $(\text{CH}_3)_3\text{Al}$, Aldrich, 97%] was used as received. Trimethylaluminum- d_9 [TMA- d_9 or $(\text{CD}_3)_3\text{Al}$] was synthesized by the reaction of aluminum powder, CD_3I , and I_2 with ultrasonic irradiation to form methyl aluminum sesquioxide that was then treated in a ligand exchange reaction with triethylaluminum and distilled to give the product, following the literature method of Yang *et al.*²⁰ In each case, the TMA was transferred to a Pyrex U-tube and degassed and pressurized with 50 psi of argon at room temperature. The argon was bubbled through the liquid TMA (room temperature vapor pressure of the predominantly dimeric species ~ 9 Torr) and the precursor gas mixture was delivered to the pulsed valve through stainless steel tubing.

III. RESULTS AND ANALYSIS

A. 3D spectra

We have used 3D LIF spectroscopy to survey the LIF spectra of the products of a trimethylaluminum/argon discharge from 14 000 to 30 000 cm^{-1} . A portion of the resulting spectrum is shown in Fig. 1, which illustrates the power of the technique for identifying fluorescent molecules in our pulsed discharge jet. The top trace shows the total LIF spectrum integrated between 0 and 7 μs after the laser pulse. The middle trace exhibits the emission spectra, presented as downward-going, color-coded intensities as a function of the scanned laser excitation wavenumber. The emission is presented as displacement (laser wavenumber–emission wavenumber, in cm^{-1}) from the laser, which gives a direct measure of the lower (typically ground state) energy of each transition. Thus, transitions at 0 cm^{-1} displacement are resonance fluorescence down to the initial vibrational level excited by the laser and a transition with a displacement of 1000 cm^{-1} would be a transition from the upper vibronic state populated by the laser to an energy level 1000 cm^{-1} above the initial vibrational level.

The bottom panel shows the fluorescence decay (in μs) at each laser wavenumber. Species with very short fluorescence lifetimes typically have an intense feature at 0 μs , which rapidly fades out before $\sim 1\text{ }\mu\text{s}$. Longer-lived species have a fluorescence tail that may persist for 2–7 μs as exhibited by the two strongest bands in the top trace.

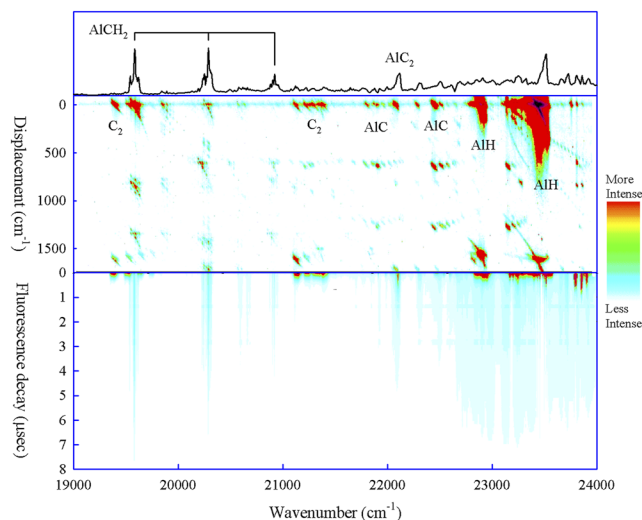


FIG. 1. A portion of the 3D LIF spectrum of the products of a discharge through a mixture of trimethylaluminum vapor and high pressure argon. In both plots, the horizontal axis is the excitation laser wavenumber (cm^{-1}). The top spectrum is the total LIF fluorescence and the middle panel is the emission spectrum obtained at each laser wavenumber (plotted as displacement in cm^{-1} from the laser) and arranged vertically. The bottom panel is the temporal profile of the fluorescence decay vs laser wavenumber. The intensities are color coded in the online version.

A thorough study of the LIF bands, their fluorescence lifetimes, and their emission spectra showed that most of the features in the spectrum could be assigned to known species, including C_2 bands, with a very short fluorescence lifetime and a vibrational interval of $\sim 1750\text{ cm}^{-1}$, along with CH, C_3 , AlC, and AlH.

The three features labeled AlCH_2 in Fig. 1 could not be assigned to any known hydrocarbon or aluminum-containing molecules. All three have similar, long-lived fluorescence lifetimes and exhibit LIF and emission patterns that are characteristic of an asymmetric top with an A value of about 10 cm^{-1} . The observed ground state vibrational intervals, the limited extent of the band system, and its onset near 19 500 cm^{-1} are all attributes predicted *ab initio* for the $\tilde{B}^2A_2 - \tilde{X}^2B_1$ band system of AlCH_2 , as summarized in Table I. Our higher resolution studies, reported below, fully support this preliminary assignment.

B. Vibrationally resolved LIF and emission spectra

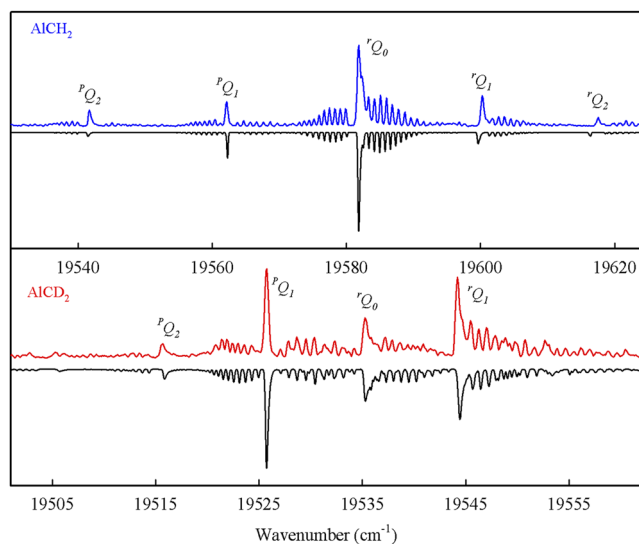
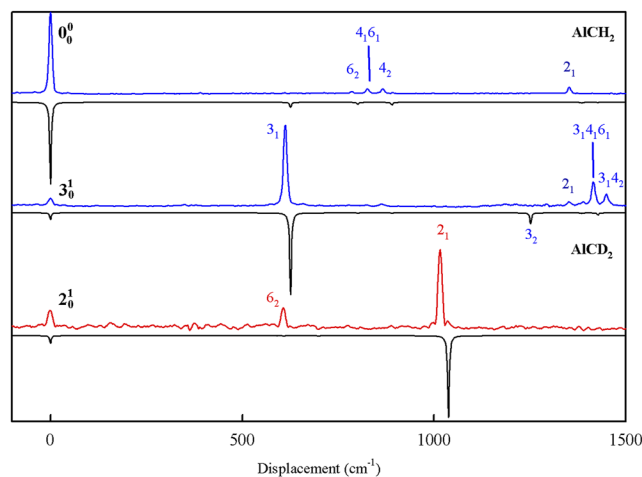
In the subsequent discussion, comparisons of the vibrational frequencies will be denoted $\text{AlCH}_2/\text{AlCD}_2$ for brevity. The first band in the LIF spectrum of AlCH_2 occurs at 19 581.9 cm^{-1} (only 167 cm^{-1} higher than the *ab initio* T_0 calculated for the $\tilde{B} - \tilde{X}$ band system¹²) and exhibits the typical rotational contour of a perpendicular band (in this case, bands following b -type selection rules) of an asymmetric top, as shown in Fig. 2. For a ground state of B_1 symmetry, the nuclear statistical weights vary according to the even (e) or odd (o) values of K_a, K_c as e, e = e, o = 3; o, o = o, e = 1 so the central rQ_0 branch would be expected to be particularly strong, as is observed. Figure 2 also shows a calculated spectrum, disregarding electron spin-rotation effects, based on the ground and excited state

TABLE I. *Ab initio* spectroscopic parameters¹² for the ground and second excited states of aluminum methylene (in cm^{-1} unless otherwise indicated).

	AlCH ₂		AlCD ₂	
	\tilde{X}^2B_1	\tilde{B}^2A_2	\tilde{X}^2B_1	\tilde{B}^2A_2
ω_1 (a_1) symm. C–H stretch	3 030.9	3 080.8	2 199.4	2 228.7
ω_2 (a_1) HCH symm. bend or scissoring	1 385.5	1 376.7	1 037.4	1 022.6
ω_3 (a_1) Al–C stretch	625.9	662.6	590.4	632.0
ω_4 (b_1) out-of-plane bend	445.2	807.3	349.3	632.2
ω_5 (b_2) C–H antisymmetric stretch	3 108.1	3 176.2	2 302.5	2 361.4
ω_6 (b_2) CH ₂ antisymmetric bend or rocking	400.7	673.9	304.3	509.5
T_0	...	19 414.6	...	19 325.5
Dipole moment (D)	0.845	0.211	0.845	0.211
Transition dipole moment (D)	...	0.260	...	0.260

molecular structures taken from our *ab initio* work¹²—the agreement is obviously very good. Deuterium substitution changes the nuclear statistical weights so that e, e = e, o = 1; o, o = o, e = 2, giving greater intensity to the pQ_1 and rQ_1 branches, precisely as observed. Transitions to the \tilde{A} and \tilde{C} excited states are predicted¹² to occur either much lower ($\tilde{A}^2A_1 - \tilde{X}^2B_1$ $T_0 = 6533 \text{ cm}^{-1}$) or much higher ($\tilde{C}^2A_1 - \tilde{X}^2B_1$ $T_0 = 26\,840 \text{ cm}^{-1}$) in energy, and both are predicted to have more extensive Franck–Condon (FC) profiles than those of the present spectrum. The spectrum simulations based on our *ab initio* data, the observed vs calculated T_0 values, the vibronic extent of the spectrum, and the ground and excited state vibrational frequencies (*vide infra*) all confirm that the observed spectrum is the $\tilde{B}^2A_2 - \tilde{X}^2B_1$ band system of the previously spectroscopically unobserved AlCH₂ free radical.

Examples of the observed and calculated single vibronic level (SVL) emission spectra for selected bands of AlCH₂ and AlCD₂ are shown in Fig. 3. The calculated spectra are Franck–Condon simulations in the strictly harmonic approximation based on our *ab initio* results, as described more fully elsewhere.¹² For AlCH₂, the calculated 0–0 band emission spectrum (Fig. 3) predicts strong emission back down to the vibrationless level, weaker 3_1^0 and 1_1^0 (not shown) transitions, a very weak 2_1^0 band, and weak 6_2^0 and 4_2^0 bands. The latter two bands would not normally be expected to have any appreciable intensity but show up due to the substantial increase in the vibrational frequencies of these nontotally symmetric modes (calc increase: $\omega_4 = 81\%$, $\omega_6 = 68\%$ for both isotopologues) on electronic excitation. Curiously, although the observed spectrum is almost as simple as predicted, transitions down

**FIG. 2.** Low resolution LIF spectra (upward going features) of the 0–0 bands of AlCH₂ (top) and AlCD₂ (bottom) along with simulations (downward going features) of the spectra based on the *ab initio* rotational constants from Ref. 12 with a rotational temperature of 30 K.**FIG. 3.** Single vibronic level emission spectra of various LIF bands of AlCH₂ and AlCD₂, plotted as displacement from the excitation laser wavenumber. The upward going spectra are the experimental data, the downward going spectra are Franck–Condon simulations of the expected spectra based on the *ab initio* results.¹² In each case, the LIF transition pumped by the laser is identified in bold-face at a displacement of 0 cm^{-1} , and the lower vibrational states of the prominent bands are labeled.

to 3_1 and 1_1 are absent and instead 2_1^0 shows up much stronger than calculated ($v_2''_{\text{obs}}/\text{calc}$: AlCH₂ = 1353/1386 cm⁻¹, AlCD₂ = 1016/1037 cm⁻¹). We note that our own Franck–Condon calculations using density functional theory methods (unpublished B3LYP) reproduce the presence of 2_1^0 and the absence of 1_1^0 but still show appreciable intensity for 3_1^0 . As predicted, 6_2^0 and 4_2^0 are observed as well as a weak unexpected $4_1^0 6_1^0$ vibronically induced band. Our general conclusion is that the FC calculations predict the gross features observed experimentally but are not reliable for the finer details, in part due to vibronic coupling complications in the excited state (*vide infra*).

The LIF spectra of each isotopologue only exhibit five bands, as predicted by our published Franck–Condon simulations¹² for the $\bar{B} - \bar{X}$ system, and consistent with a small change in the molecular geometry on electronic excitation. The higher LIF bands of AlCH₂ and AlCD₂ are shown in Fig. 4. These were assigned based on a comparison of the observed and calculated vibrational intervals, their deuterium isotope effects, their subband structure, and the observed and calculated single vibronic level emission spectra. The data and assignments of the LIF and emission spectra are summarized in Tables II and III. We conclude that the first AlCH₂ band in Fig. 4, +650.4 cm⁻¹ above the 0–0 band (v_3' calc = 662.6 cm⁻¹), is 3_1^0 . Deuteration shifts the corresponding band to +623.6 cm⁻¹ above T_0 , slightly above the first AlCD₂ band in Fig. 4, giving an Al–C stretching isotope shift of 26.8 cm⁻¹, comparable to the 30.6 cm⁻¹ *ab initio* value. The emission spectra of both isotopologues show a very weak 3_0^0 band and a very strong 3_1^1 transition (see Fig. 3) with $v_3'' = 612/564$ cm⁻¹ (*ab initio* = 626/590 cm⁻¹) and an intensity distribution similar to our Franck–Condon prediction. Finally, the 0–0 and 3_0^0 Q-branch wavenumbers were fitted to the simple symmetric top formula,²¹

$$\tilde{\nu} = \nu_0 + (A - \bar{B})' (\pm 2K_a'' + 1) + [(A - \bar{B})' - (A - \bar{B})''] K_a''^2, \quad (1)$$

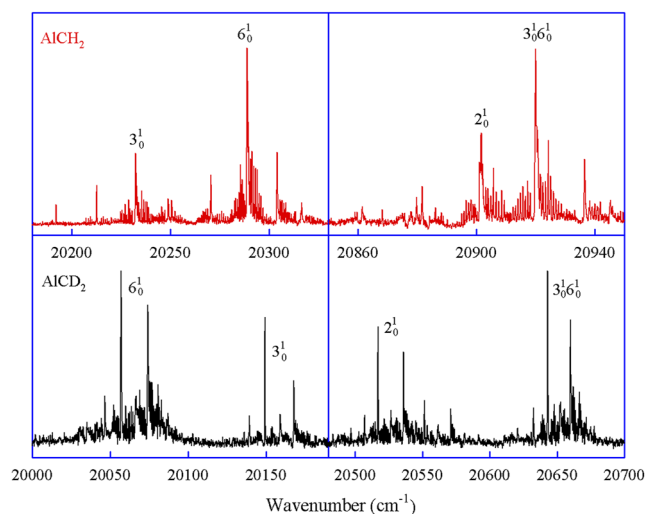


FIG. 4. The LIF spectra of AlCH₂ and AlCD₂ above the 0–0 bands with vibronic assignments.

and ν_0 , $(A - \bar{B})''$, and $(A - \bar{B})'$ (both quantities approximately equal to the A values since \bar{B} is rather small) were determined by least-squares fitting, with the results tabulated in Table II. It is apparent that the lower and upper state $A - \bar{B}$ values are similar for both transitions. Through a process of elimination, the second AlCH₂ LIF band in Fig. 4 is assigned as 6_0^1 . Emission spectroscopy shows that it is not a hot band and it occurs +707 cm⁻¹ above the 0–0 band. Since the smallest calculated vibrational frequency is $\nu_3 = 662.6$ cm⁻¹, this interval is too small to be a vibrational combination, so it must be a fundamental and the only candidate is calculated at 673.9 cm⁻¹. The value of $(A - \bar{B})'$ for this band is 1.06 cm⁻¹ smaller than that of the 0–0 band, signaling either a perturbation or a significant change in geometry. Similar results are found on deuteration, although now 6_0^1 is the first AlCD₂ band in Fig. 4. The vibrational interval from the 0–0 band drops to +531 cm⁻¹ and the isotope shift is 176 cm⁻¹, comparable to a calculated value of 164.4 cm⁻¹. The AlCD₂ $(A - \bar{B})'$ value is also significantly lower than that of the 0–0 band. All indications are that the bands at AlCH₂ = 20288.9 and AlCD₂ = 20066.4 cm⁻¹ must have the same 6_0^1 assignment. These bands would normally be forbidden but must gain intensity through a vibronic coupling mechanism.

The third AlCH₂ band in Fig. 4 is readily assigned at 2_1^0 , with an observed interval of +1319.7 cm⁻¹, somewhat lower than the 1376.7 cm⁻¹ calculated value. Deuteration reduces this frequency to +991.1 cm⁻¹ (calc = 1022.6 cm⁻¹) giving an isotope shift of 328.6 cm⁻¹ very similar to the *ab initio* prediction of 354.1 cm⁻¹. The $2_1^0(A - \bar{B})'$ value is very similar to that of the 0–0 and 3_0^0 bands. Finally, our Franck–Condon simulations suggest that the 2_1^0 band emission spectra should exhibit a very weak 2_0^1 band and a prominent 2_1^1 band, precisely as observed (see the AlCD₂ data in Fig. 3).

The final LIF bands appear at +1338.1/+1116.9 cm⁻¹ and exhibit small $(A - \bar{B})'$ values similar to those of the 6_0^1 bands, suggesting a combination with ν_6' . The $3_1^0 6_0^1$ assignment leads to intervals of $3_0^0 + 687.7/+493.2$ cm⁻¹, both suggesting a substantial anharmonicity. The emission spectra show weak resonance fluorescence and a stronger transition down to ν_3'' , as expected from our Franck–Condon simulations for an upper state level involving ν_3' .

C. High resolution rotationally resolved spectra

High resolution LIF spectra were recorded for the 0–0 bands of both isotopologues. The laser linewidth, as measured from the widths of the I₂ calibration lines, was 0.03–0.035 cm⁻¹, but the aluminum methylene LIF linewidths were typically 0.04–0.05 cm⁻¹, even when the laser power was attenuated to eliminate broadening. The spectra were scanned in segments of 10–20 cm⁻¹ and each calibrated individually to an overall standard deviation of 0.0027–0.0035 cm⁻¹ by fitting the individual I₂ LIF lines to a Gaussian function. The reproducibility of measuring single, well-resolved LIF lines was ~0.008 cm⁻¹.

It was immediately apparent that every rotational line in Fig. 2 was split into two lines at high resolution, as shown in Fig. 5. Asymmetric top free radicals generally belong to Hund's case (b), and, in the absence of large hyperfine effects, the spin–rotation interaction

TABLE II. Assignments and central rQ_0 branch maxima (cm^{-1}) of the observed bands in the LIF spectra of AlCH_2 and AlCD_2 .

Assign.	AlCH_2			AlCD_2		
	rQ_0	Comment ^a	<i>Ab initio</i> ¹²	rQ_0	Comment	<i>Ab initio</i> ¹²
0_0^0	19 581.9	$A'' = 10.026$ $A' = 9.505$	19 414.6	19 535.4	H/D shift = -46.5 $A'' = 4.902$ $A' = 4.631$	H/D shift = -89.1 19 325.5
3_0^1	20 232.3	$A'' = 10.037$ $A' = 9.470 + 650.4$	$\nu_3 = 662.6$	20 159.0	$A'' = 4.909$ $A' = 4.6450 + 623.6$	$\nu_3 = 632.0$
6_0^1	20 288.9	$A'' = 10.006$ $A' = 8.445 + 707.0$	$\nu_6 = 673.9$	20 066.4	$A'' = 4.901$ $A' = 4.265 + 531.0$	$\nu_6 = 509.5$
2_0^1	20 901.6	$A'' = 10.055$ $A' = 9.865 + 1319.7$	$\nu_2 = 1 376.7$	20 526.5	$A'' = 4.879$ $A' = 4.749 + 991.1$	$\nu_2 = 1 022.6$
$3_0^1 6_0^1$	20 920.0	$A'' = 10.040$ $A' = 8.893$ Perturbed $3_0^1 + 687.7$		20 652.3	$A'' = 4.958$ $A' = 4.265$ Perturbed $3_0^1 + 493.2$	

^aThe constants are actually $(A - \bar{B})'' \approx A''$ and $(A - \bar{B})' \approx A'$ values [see Eq. (1)].

is by far the most important contributor to the fine structure. The vector coupling is termed case (b_{βj})²² and is given by

$$\mathbf{N} + \mathbf{S} = \mathbf{J} \quad \mathbf{J} + \mathbf{I} = \mathbf{F}. \quad (2)$$

We then label the rotational levels of each vibronic state by N_{K_a, K_c} , J where N is the rotational angular momentum quantum number,

K_a and K_c are the usual asymmetric top labels, and $J = N \pm S$ ($S =$ electron spin quantum number of $1/2$) is the quantum number for the total angular momentum including electron spin but excluding nuclear spin. Conventionally, a state with $J = N + 1/2$ is labeled F_1 and $J = N - 1/2$ is F_2 . Further hyperfine effects (if observable) can be accommodated with the quantum number $F = J + I, J + I - 1, \dots, |J - I|$.

TABLE III. Observed vibrational levels of the \tilde{X}^2B_1 state of AlCH_2 and AlCD_2 (in cm^{-1} relative to the zero-point level).

AlCH_2				AlCD_2			
Level	Energy	Theory ^a	Spectrum (int.) ^b	Level	Energy	Theory ^a	Spectrum (int.) ^b
3_1	612	626	$3_0^1(s), 3_0^1 6_0^1(m)$	3_1	564	590	$3_0^1(s), 3_0^1 6_0^1(m)$
6_2	784	801	$0-0(w), 2_0^1(w)$	6_2	608	609	$0-0(w), 2_0^1(w)$
$4_1 6_1$	826	846	$0-0(w)$	$4_1 6_1$	642	653	$0-0(w)$
4_2	866	890	$0-0(w), 2_0^1(w), 3_0^1 6_0^1(w)$	4_2	689	699	$0-0(m), 2_0^1(w), 3_0^1 6_0^1(w)$
2_1	1353	1386	$2_0^1(s), 0-0(w), 3_0^1(w)$	2_1	1016	1037	$2_0^1(s), 0-0(w), 3_0^1(w)$
...	3_2	1117	1180	$6_0^1(w)$
$3_1 4_1 6_1$	1415	1438	$3_0^1(m), 6_0^1(w)$
$3_1 4_2$	1450	1516	$3_0^1(w), 6_0^1(w)$	$3_1 4_2$	1226	1289	$6_0^1(m), 3_0^1(w)$
$4_3 6_1$	1703	1736	$6_0^1(s), 3_0^1(w)$	$3_2 6_1$	1411	1485	$6_0^1(m), 3_0^1 6_0^1(w), 3_0^1(w)$
$2_1 6_1$	1751	1787	$6_0^1(m)$
$2_1 3_1$	1962	2012	$3_0^1(m)$	$2_1 3_1$	1578	1627	$3_0^1(w)$
...	$2_1 6_2$	1624	1646	$2_0^1(w)$
$3_3 6_1$	2234	2279	$6_0^1(w)$	$2_1 4_1 6_1$	1656	1690	$3_0^1 6_0^1(m)$
				$2_1 4_2$	1717	1736	$2_0^1(w)$
				$3_2 4_2?$	1765	1879	$3_0^1 6_0^1(m)$
				$3_1 4_4?$	1921	1988	$3_0^1 6_0^1(m)$
				2_2	2020	2074	$2_0^1(m)$

^aReference 12. For combination or overtone levels, the numbers quoted are sums of the vibrational fundamentals.

^bThe emission spectrum in which the ground state interval appears and relative intensity (s = strong, m = medium, w = weak) of the transition to that level in the spectrum.

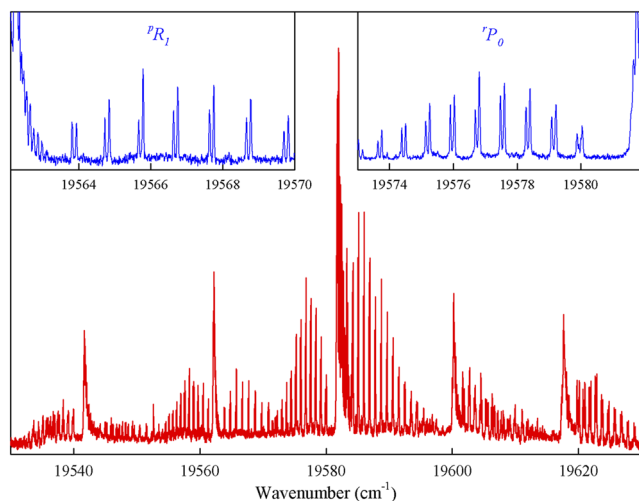


FIG. 5. The high resolution LIF spectrum of AlCH_2 . The insets show the ${}^{\rho}R_1$ and ${}^{\rho}P_0$ branches illustrating the splittings found in each branch of the spectrum.

Initially, we assumed that the doublets in the spectrum are due to the spin–rotation splittings in the ground and excited states. We crudely estimated the major ε_{aa} spin–rotation constant based on the pure precession relationship (considering only the \tilde{X} and \tilde{B} states),²³

$$\varepsilon_{aa} \approx \frac{\pm 4A\zeta_{3p}}{\Delta E}, \quad (3)$$

where A is the rotational constant, taken from the simulation in Fig. 2, ζ_{3p} is the spin–orbit coupling constant of the Al atom (74.7 cm^{-1}),²³ ΔE is the vertical excitation energy (taken as the observed ${}^{\rho}Q_0$ branch maximum of the 0_0^0 band = 19582 cm^{-1}), and the \pm signs are for the excited and ground states, respectively. These yield $\varepsilon_{aa}'' = -0.16$ and $\varepsilon_{aa}' = +0.15 \text{ cm}^{-1}$. Although the absolute magnitudes are likely in error, the signs should be reliable.

Since the signs of the major spin–rotation constant ε_{aa} are expected to be opposite, $F_2 > F_1$ in the ground state and $F_1 > F_2$ in the excited state. The $F_1 - F_1$ and $F_2 - F_2$ transitions are expected to be the most prominent and the resultant spin splitting in the spectrum is the sum of the upper and lower state spin splittings. The choice of assignment, irrespective of the actual signs of the ε_{aa} constants, was based on intensities. Since the Boltzmann and nuclear statistical weightings are almost identical for the F_1 and F_2 levels of the same N'' , the greater intensity comes from the degeneracy ($2J + 1$), which is larger for the F_1 component. Thus, we initially assigned the more intense transitions in the ${}^{\rho}P_0$ and ${}^{\rho}R_0$ branches of the upper spectrum in Fig. 5 as $F_1 - F_1$. In this fashion, assignments of the uncomplicated $K'_a = 1 - K''_a = 0$ and $K'_a = 0 - K''_a = 1$ subbands were made.

In the instance of the $K'_a = 1 - K''_a = 2$ and $K'_a = 2 - K''_a = 1$ subbands, the rotational structure is somewhat more intricate due to the effects of asymmetry in the $K_a = 1$ levels. In this case, each level is split into two asymmetry components, so there will be a total of four transitions for each value of N'' . It is found in the present spectra that the splittings are relatively constant with N , but the asymmetry splittings increase with N in the manner typical of a prolate

asymmetric top. Assignments were made by simulating the spectrum with the PGOPHER program²⁴ and varying the rotational and spin constants until it matched the experimental spectrum well enough to identify individual lines. Most of the Q-branch lines were overlapped or otherwise compromised, so very few reliable $\Delta N = 0$ assignments were available.

It soon became apparent that fitting the doublets in the spectrum as spin–rotation splittings was fraught with difficulties. It was possible to fit portions of the spectrum but not all of it and there were always systematic residuals that suggested a fundamental problem with this approach.

This situation was reminiscent of our previous rotational analysis of the $B^4\Sigma^- - X^4\Sigma^-$ bands of AlCl , where we showed that the observed splittings of the rotational lines are due to the Fermi contact hyperfine interaction in the excited state rather than the expected electron spin–spin coupling.¹⁷

Four specific aspects of the AlCH_2 spectrum reinforced our suspicion that the observed splittings had a hyperfine origin. First, the unpaired electron is in a p -type orbital on aluminum in the ground state, with negligible Fermi contact effect, but is in an s -type aluminum orbital in the excited state, with a potentially substantial Fermi contact interaction (see Fig. 3 of Ref. 12). Second, the observed splittings (0.12 – 0.14 cm^{-1}) in various branches with $K'_a \leq 2$ are fairly constant independent of N and are not substantially different in AlCH_2 and AlCD_2 , contrary to expectations for spin–rotation effects. Third, as shown in Fig. 6, some of the rotational lines exhibit asymmetric, triangular shapes, consistent with unresolved hyperfine structure. Finally, Fig. 6 shows that the AlCH_2 ${}^{\rho}P_0(2)$ doublet exhibits further small splittings that would only be explainable as hyperfine effects.

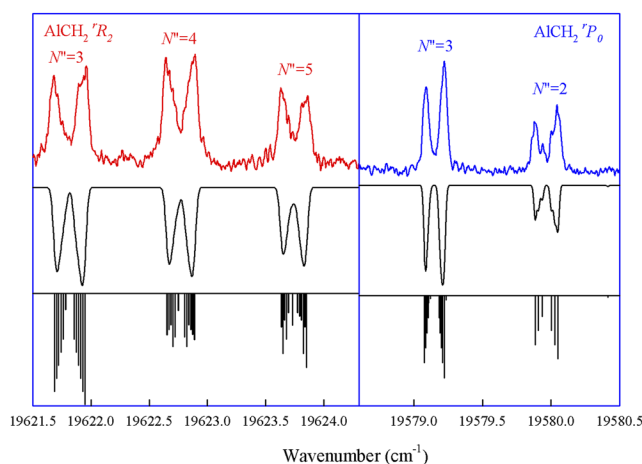


FIG. 6. Selected lines in the high resolution spectrum of AlCH_2 . In each case, the observed spectrum is at the top and calculated downward spectra below. The left hand panel shows lines of the ${}^{\rho}R_2$ branch, which exhibit triangular profiles. Directly below is the spectrum calculated using the constants of Table IV and a linewidth of 0.045 cm^{-1} . The right hand panel shows the beginning of the ${}^{\rho}P_0$ branch with additional structure in the first member. Directly below it is the calculated spectrum with a linewidth of 0.023 cm^{-1} . The bottom trace in each panel is the calculated hyperfine structure with a linewidth a factor of 10 smaller than the middle trace.

If the nuclear spin and electron spin are strongly coupled [case ($b_{\beta S}$) coupling²²], then

$$\mathbf{G} = \mathbf{I} + \mathbf{S} \text{ and } \mathbf{F} = \mathbf{N} + \mathbf{G}. \quad (4)$$

Since the quantum numbers are $I = 2.5$ for ^{27}Al and $S = 0.5$, each upper state rotational level is split into two components with $G = 3$ and 2 and relative energies,

$$E_G = 0.5a_F[G(G+1) - I(I+1) - S(S+1)], \quad (5)$$

where a_F is the polyatomic Fermi contact parameter. To the first approximation, the separation of the doublets is

$$\Delta E_{G=3-G=2} \approx 0.12 \text{ cm}^{-1} = 0.5a_F[3(3+1) - 2(2+1)] = 3a_F, \quad (6)$$

which yields $a_F \approx 0.04 \text{ cm}^{-1}$. A simulation of the AlCH_2 spectrum using the rotational constants and band origin obtained from our preliminary work (which assumed spin-rotation splittings) and only $a'_F = 0.04 \text{ cm}^{-1}$ gave very good agreement with experiment at low values of K'_a . At this level of approximation, all the F components of each G level are degenerate so there is no further splitting of the ${}^rP_0(2)$ doublet (see Fig. 6), contrary to observation. Furthermore, the asymmetric triangular lineshapes and larger splittings ($0.39\text{--}0.17 \text{ cm}^{-1}$) of the rR_2 branch (Fig. 6) are not satisfactorily modeled without additional contributions. Reasoning that a secondary spin-rotation interaction would lift the F quantum number degeneracy and modify the splittings, we found that $\epsilon'_{aa} \approx 0.1 \text{ cm}^{-1}$ gave a very satisfactory simulation.

The hyperfine coupling scheme used in the PGOPHER program²⁴ is $\mathbf{J} = \mathbf{N} + \mathbf{S}$ and $\mathbf{F} = \mathbf{J} + \mathbf{I}$ [case ($b_{\beta J}$)] so it was necessary to denote assignments with the N , K_a , K_c , J , and F quantum numbers for each of the combining states. A set of initial AlCH_2 assignments were made, attributing the observed transition to the most intense F component in each case, except for the more complex hyperfine-split ${}^rP_0(2)$ doublet. An effective Hamiltonian of the form

$$H_{\text{eff}} = H_{\text{rot}} + H_{\text{cd}} + H_{\text{sr}} + H_{\text{hfs_Al}}, \quad (7)$$

was used to fit the transitions, as implemented in the PGOPHER program. Here, H_{rot} and H_{cd} refer to the rotational energy and its

centrifugal distortion corrections, H_{sr} is the spin-rotation interaction, and $H_{\text{hfs_Al}}$ is the Fermi contact hyperfine term for the aluminum atom.

As suggested by our preliminary simulations, we initially fitted the rotational constants A , B , and C in both states, the band origin T_0 , the excited state Fermi contact constant aF' , and the excited state spin-rotation constant ϵ'_{aa} . Since the data extended up to $N = 15$ in both states and $K'_a = 3$, the centrifugal distortion constants Δ''_{JK} , Δ'_{JK} , and Δ'_K were also determinable. The ground state spin-rotation constants and excited state ϵ_{bb} and ϵ_{cc} could not be determined and were fixed at values of 0.0 cm^{-1} . In the final least squares analysis, 199 individual AlCH_2 transitions with equal weights were fitted with 12 constants to an overall standard deviation of 0.0048 cm^{-1} , well within the experimental error.

In the analysis of the high-resolution spectrum of AlCD_2 , we simulated the spectrum using rotational constants, a'_F equal to that of AlCH_2 , and a spin-rotation constant ϵ'_{aa} scaled by the A' values of the two isotopologues [Eq. (2)], which corresponded very well to experiment and permitted assignments to be made. In this case, there were more overlapping lines, the spectra were weaker, and they extended to higher K_a values ($K'_a = 4$, $K''_a = 3$) so it was necessary to add an additional Δ'_K constant to get a satisfactory fit of all the branches. In the final analysis, 240 lines were fitted with an overall standard deviation of 0.0055 cm^{-1} , slightly larger than that of AlCH_2 due to the more extensive line overlap. The fitted molecular constants for AlCH_2 and AlCD_2 are summarized in Table IV and simulations of portions of the spectra based on these constants are shown in Fig. 7. Detailed lists of assignments and calculated values are given in the supplementary material.

IV. DISCUSSION

A. The molecular structure of AlCH_2

The molecular structures of AlCH_2 in the combining electronic states were derived from the rotational constants of AlCH_2 and AlCD_2 as given in Table IV. The small positive inertial defects ($\text{AlCH}_2 \tilde{X} = 0.088 \text{ amu } \text{\AA}^2$, $\tilde{B} = 0.041 \text{ amu } \text{\AA}^2$) and the results of previous *ab initio* work¹² suggest that aluminum methylene is planar in both states. The effective (r_0) structures were determined by a least squares fit to the planar moments of inertia, Pa and Pb , calculated

TABLE IV. The molecular constants (in cm^{-1}) of AlCH_2 and AlCD_2 .^a

Parameter	\tilde{X}^2B_1		\tilde{A}^2A_2	
	$\text{AlCH}_2 0_0$	$\text{AlCD}_2 0_0$	$\text{AlCH}_2 0^0$	$\text{AlCD}_2 0^0$
T_0	19 572.16092(96)	19 530.429 27(90)
A	10.441 68(41)	5.230 08(54)	9.912 11(66)	4.984 43(35)
B	0.427 972(38)	0.365 059(32)	0.438 266(30)	0.375 684(33)
C	0.410 244(36)	0.340 157(32)	0.419 287(27)	0.348 968(34)
Δ_K	...	$1.53(52) \times 10^{-4}$	$8.37(69) \times 10^{-4}$	$2.35(19) \times 10^{-4}$
Δ_{JK}	$6.84(58) \times 10^{-5}$	$4.42(39) \times 10^{-5}$	$4.94(42) \times 10^{-5}$	$1.08(25) \times 10^{-5}$
ϵ_{aa}	0.103 3(18)	0.034 8(14)
a_F (Al)	0.037 44(26)	0.038 77(30)

^aThe numbers in parentheses are 1σ error limits.

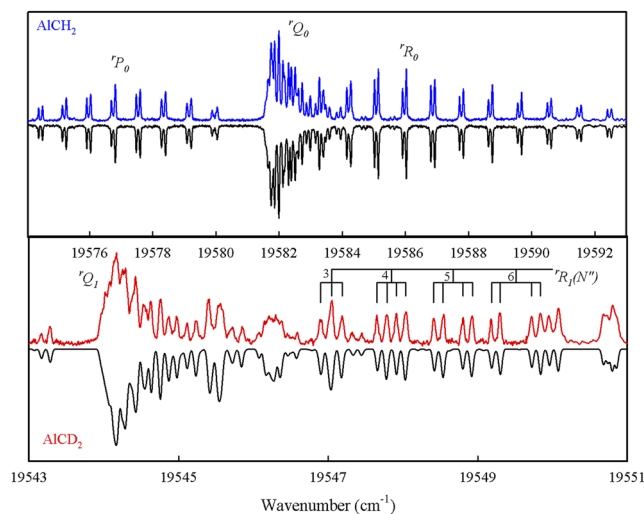


FIG. 7. Portions of the high resolution LIF spectra of AlCH_2 (top) and AlCD_2 (bottom) along with simulations based on the constants in Table IV, linewidths of 0.045 cm^{-1} , and rotational temperatures of 30 K. The assignments of the hyperfine- and asymmetry-split $r'_i(N)$ branch of AlCD_2 are indicated. The hyperfine-splittings are denoted by vertical leaders of the same length and are relatively constant whereas the asymmetry splittings increase with N . In each case, the lower wavenumber component involves $G' = 2$, and the higher wavenumber feature $G' = 3$.

from the rotational constants and weighted as the inverse square of the uncertainties. The third planar moment, P_c , was omitted from the analysis as the planarity condition constrains it to zero, although the actual values were of the order of -0.07 to $-0.02 \text{ amu } \text{\AA}^2$ due to the nonzero inertial defect. A 0.003 \AA contraction of the C–H bond length on deuteration (Laurie correction)²⁵ was included in the structure determination. The resulting structures are presented in Table V, along with our *ab initio* predictions.¹² The theoretical results are in good agreement with the experimental values, although the theory overestimates the Al–C bond length in both states. A similar phenomenon was found for the ground state of AlC , where a variety of *ab initio* calculations overestimated the r_e bond length by 0.01 – 0.02 \AA , but our systematic extrapolation to the complete basis set limit and the inclusion of core correlation reduced the discrepancy to 0.0005 \AA .¹⁷

The present Al–C bond lengths (1.959 – 1.943 \AA) can be compared to the corresponding ground state bond lengths of AlC : $r_e = 1.9557(1) \text{ \AA}$ (Ref. 17), AlCCH : $r_0 = 1.963(5) \text{ \AA}$ (Ref. 26), AlCH_3 : $r_0 \approx 1.98 \text{ \AA}$ (Ref. 27), and $\text{Al}(\text{CH}_3)_3 = 1.957(3) \text{ \AA}$ (Ref. 28), all

TABLE V. Experimental and *ab initio* geometric parameters of AlCH_2 .

Parameter	\tilde{X}^2B_1		\tilde{B}^2A_2	
	Expt. (r_0)	Theory (r_e)	Expt. (r_0)	Theory (r_e)
r_{AlC} (\AA)	1.959(1)	1.9766	1.943(1)	1.9546
r_{CH} (\AA)	1.106(1)	1.0953	1.091(1)	1.0884
θ_{HCH} (deg)	110.4(1)	110.0	115.4(1)	114.2

obtained from gas phase spectroscopic studies. The bond lengths are all very similar and are characteristic of aluminum–carbon single bonds, which has been the theoretical prediction for AlCH_2 since the 1982 work of Cook and Allen.⁸ It is also apparent that the geometric structure does not change substantially on electronic excitation, as predicted¹² for a transition that involves the promotion of an electron from the $7a_1$ (Al 3s nonbonding) to the $3b_2$ (Al in-plane 3p nonbonding) molecular orbital.

B. Rotational and vibrational analysis

The data in Table III show that the measured ground state vibrational frequencies of AlCH_2 and AlCD_2 are, as expected, comparable to but slightly smaller than the *ab initio* values. Unfortunately, there are not enough data to use the Teller–Redlich product rule²⁹ to test the validity of the vibrational assignments. However, the H/D isotope effects, the general correspondence between the observed and Franck–Condon simulations of the emission spectra, and the observation that excited state vibrational levels tend to emit strongly down to similar vibrational levels (a general rule of thumb that is often followed), all support the validity of our ground state frequencies. Of particular interest is the AlCH_2 experimental $\nu_4'' = 433 \text{ cm}^{-1}$ (taken as half the frequency of the 4_2 level), in good accord with our ICMRCI/aug-cc-pVTZ *ab initio* value (445.2 cm^{-1})¹² but very different from the previous coupled cluster singles, doubles and perturbative triples [CCSD(T)] with a cc-pwCVQZ basis set value of $\nu_4'' = 659 \text{ cm}^{-1}$ fundamental, reported in a calculation that suffered from SCF instability problems.²

The excited state energy levels and LIF transition frequencies of $\text{AlCH}_2/\text{AlCD}_2$ are reported in Table II. The subband analysis gives approximate values of A'' and A' for each band, showing that the 0_0^0 , 3_0^1 and 2_0^1 bands terminate on upper state levels with similar A values, whereas the 6_0^1 and $3_1^1 6_0^1$ bands have substantially smaller A' values, signaling a distortion of the molecular structure along the Q_6 normal coordinate. This is consistent with the fact that the ν_6' frequencies are slightly larger than the *ab initio* values. On the basis of the vibrational frequencies, isotope shifts, and emission spectra, the assignments involving ν_6' seem secure, although the exact mechanism by which these forbidden components of the allowed transition occur is as yet unclear.

The analysis of the high-resolution spectra turned out to be much more interesting than anticipated. The excited state is one of the very few examples of an asymmetric top free radical whose fine structure follows case (b_{gs}) coupling with splittings that are primarily due to a substantial aluminum Fermi contact interaction rather than the usual spin–rotation effects. In fact, the ground state spin–rotation constants, which were expected to be significant [Eq. (2)], were not determinable from the present data.

The Fermi contact parameters of both isotopologues (Table IV) are sensibly similar, as they must be since the electronic wavefunction is isotope independent. Since only s electron wavefunctions have nonzero amplitude at the nucleus, the Fermi contact parameter is a measure of the unpaired s electron spin density, in this case involving the aluminum 3s electron. The percentage of Al 3s character in the $7a_1$ molecular orbital (MO) may be obtained from the ratio of the molecular Fermi contact parameter, a_F , to that of a single electron in the aluminum atomic 3s orbital, b_F (Al 3s). Using the Morton

and Preston³⁰ *ab initio* atomic value of b_F (Al 3s) = 3911 MHz (0.1305 cm^{-1}), an average $a_F = 0.0381 \text{ cm}^{-1}$ for $\text{AlCH}_2/\text{AlCD}_2$ yields 29.2% 3s character for the $7a_1$ MO.

The excited state spin-rotation constants ϵ'_{aa} do not follow the isotope relations very well, as they should be in the ratio of the A' values ($A_D/A_H = 0.50$) whereas $\epsilon_{aa}(D)/\epsilon_{aa}(H) = 0.34$. This is a bit disconcerting but it must be remembered that the ϵ_{aa} values are primarily determined from a very limited set of weak and broad transitions [${}^1P_0(2)$ and the 1R_2 branch in the case of AlCH_2 —see Fig. 6] and so are probably less well defined than their statistical errors suggest. The lack of any determinable spin-rotation effects attributable to the ground state suggests that these constants must be quite small.

V. CONCLUSIONS

With the aid of our own high-level *ab initio* predictions,¹² the aluminum methylene free radicals have been observed spectroscopically for the first time. The electronic transition, detected by laser-induced fluorescence spectroscopy in the 513–483 nm region, is assigned as the $\tilde{B}^2A_2 - \tilde{X}^2B_1$ band system. LIF and single vibronic level emission studies have identified ν_2 , ν_3 , and ν_6 in the excited state and ν_2 , ν_3 , ν_4 , and ν_6 in the ground state and show that the upper state is affected by vibronic coupling with other nearby excited states. High-resolution, rotationally resolved spectra have been obtained for the 0–0 bands of AlCH_2 and AlCD_2 , which show resolved splittings in all branches due to the presence of the unpaired electron. The analysis yielded the rotational constants from which molecular structures were derived for the combining states.

SUPPLEMENTARY MATERIAL

See the [supplementary material](#) for (I) a list of the observed and calculated transition frequencies, assignments, and least squares results for the high resolution 0–0 band spectrum of AlCH_2 and (II) a list of the observed and calculated transition frequencies, assignments, and least squares results for the high resolution 0–0 band spectrum of AlCD_2 .

ACKNOWLEDGMENTS

We thank Tim Steimle of Arizona State University for sharing the details of his 2D LIF spectrometer with us. We also express our gratitude to Gretchen Rothschof for her early contributions to this project and to Joseph Cardon for his help with the high-resolution laser. This research was funded by Ideal Vacuum Products.

AUTHOR DECLARATIONS

Conflict of Interest

The authors have no conflicts to disclose.

Author Contributions

Fumie X. Sunahori: Formal analysis (equal); Writing – review & editing (equal). **Tony C. Smith:** Conceptualization (equal);

Funding acquisition (equal); Writing – review & editing (equal). **Dennis J. Clouthier:** Conceptualization (equal); Data curation (equal); Formal analysis (equal); Writing – original draft (equal).

DATA AVAILABILITY

The data that support the findings of this study are available within the article and its [supplementary material](#).

REFERENCES

- 1 M. N. Sudheendra Rao, H. W. Roesky, and G. Anantharaman, *J. Organomet. Chem.* **646**, 4 (2002).
- 2 K. R. Compaan, J. Agarwal, B. E. Dye, Y. Yamaguchi, and H. F. Schaefer III, *Astrophys. J.* **778**, 125 (2013).
- 3 A. Janczyk and L. M. Ziurys, *Astrophys. J., Lett.* **639**, L107 (2006).
- 4 J. M. Hollis, P. R. Jewell, and F. J. Lovas, *Astrophys. J.* **438**, 259 (1995).
- 5 Wikipedia, List of interstellar and circumstellar molecules, https://en.wikipedia.org/wiki/List_of_interstellar_and_circumstellar_molecules and references therein, 2022.
- 6 R. Srinivas, D. Suelzle, and H. Schwarz, *J. Am. Chem. Soc.* **112**, 8334 (1990).
- 7 D. J. Fox, D. Ray, P. C. Rubesin, and H. F. Schaefer III, *J. Chem. Phys.* **73**, 3246 (1980).
- 8 C. M. Cook and L. C. Allen, *Organometallics* **1**, 246 (1982).
- 9 S. Q. Jin, Y. Xie, and H. F. Schaefer III, *Chem. Phys. Lett.* **170**, 301 (1990).
- 10 S. Q. Jin, Y. Xie, and H. F. Schaefer III, *J. Chem. Phys.* **95**, 1834 (1991).
- 11 C. J. Cramer, *J. Mol. Struct.* **235**, 243 (1991).
- 12 R. Tarroni and D. J. Clouthier, *J. Chem. Phys.* **153**, 014301 (2020).
- 13 W. W. Harper, E. A. Ferrall, R. K. Hilliard, S. M. Stogner, R. S. Grev, and D. J. Clouthier, *J. Am. Chem. Soc.* **119**, 8361 (1997).
- 14 W. W. Harper, K. W. Waddell, and D. J. Clouthier, *J. Chem. Phys.* **107**, 8829 (1997).
- 15 D. L. Michalopoulos, M. E. Geusic, P. R. R. Langridge-Smith, and R. E. Smalley, *J. Chem. Phys.* **80**, 3556 (1984).
- 16 J. Yang, R. H. Judge, and D. J. Clouthier, *J. Chem. Phys.* **135**, 124302 (2011).
- 17 D. J. Clouthier and A. Kalume, *J. Chem. Phys.* **144**, 034305 (2016).
- 18 M. Gharaibeh and D. J. Clouthier (unpublished).
- 19 S. Gerstenkorn and P. Luc, *Atlas du Spectre D'Absorption de la Molecule d'Iode* (Editions du CNRS, Paris, 1978); S. Gerstenkorn and P. Luc, *Rev. Phys. Appl.* **14**, 791 (1979).
- 20 P.-H. Yang, K.-F. Liou, and Y.-T. Lin, *J. Organomet. Chem.* **307**, 273 (1986).
- 21 G. Herzberg, *Molecular Spectra and Molecular Structure* (Van Nostrand, New York, 1966), Vol. II, p. 424.
- 22 C. H. Townes and A. L. Schawlow, *Microwave Spectroscopy* (Dover, New York, 1975).
- 23 H. Lefebvre-Brion and R. W. Field, *Perturbations in the Spectra of Diatomic Molecules* (Academic Press, Orlando, 1986), p. 214.
- 24 C. M. Western, "PGOPHER: A program for simulating rotational, vibrational and electronic spectra," *J. Quant. Spectrosc. Radiat. Transfer* **186**, 221–242 (2016).
- 25 V. W. Laurie and D. R. Herschbach, *J. Chem. Phys.* **37**, 1687 (1962).
- 26 M. Sun, D. T. Halfen, J. Min, D. J. Clouthier, and L. M. Ziurys, *Chem. Phys. Lett.* **553**, 11 (2012).
- 27 J. S. Robinson and L. M. Ziurys, *Astrophys. J.* **472**, L131 (1996).
- 28 A. Almennigen, S. Halvorsen, and A. Haaland, *Acta Chem. Scand.* **25**, 1937 (1971).
- 29 G. Herzberg, *Molecular Spectra and Molecular Structure* (Van Nostrand, New York, 1966), Vol. II, p. 231.
- 30 J. R. Morton and K. F. Preston, *J. Magn. Reson.* **30**, 577 (1978).